

## Use of spin-polarized electron-energy-loss spectroscopy to investigate dipole and impact scattering from transition-metal surfaces

H. Hsu, M. Magumela, B. E. Johnson, F. B. Dunning, and G. K. Walters

*Department of Physics and the Rice Quantum Institute, Rice University, 6100 S. Main Street, Houston, Texas 77005*

(Received 25 November 1996)

Spin polarized electron-energy-loss spectra have been obtained from Ag(100), Cu(100), Mo(110) and unmagnetized Co(110) and Fe(100) surfaces, in both specular and off-specular scattering geometries, by use of a low-energy polarized incident beam coupled with energy- and angle-resolved spin analysis of the scattered electrons. The data are interpreted in terms of a model that takes account of both dipole and impact scattering. Dipole scattering preserves the full polarization of the incident beam, whereas the scattered electron polarization is degraded by electron exchange in impact-scattering events that produce electron-hole pair excitation in the target. It is found that dipole scattering dominates at noble-metal surfaces but that the impact- and dipole-scattering rates are comparable for targets with incompletely filled *d* shells. The data also suggest that impact scattering, like dipole scattering, tends to be concentrated in the specular direction. [S0163-1829(97)04720-6]

### I. INTRODUCTION

Electron-energy-loss spectroscopy is used extensively in the study of elementary electronic excitations at crystalline surfaces. For low-energy ( $\leq 100$  eV) electrons incident upon an atomically clean metal surface, excitation of intra- and interband transitions and of surface plasmons generally provides the dominant source of inelastically backscattered electrons for energy losses extending up to  $\sim 10$  eV or more. These mechanisms result in a broad, relatively featureless energy-loss spectrum. Inelastic energy loss can occur either in the vacuum outside the target surface (termed dipole scattering), or upon penetration of the target (termed impact scattering). Electrons undergoing these different types of inelastic scattering are superimposed in the observed electron-energy-loss spectrum and their separate contributions to the total inelastically scattered electron signal are impossible to determine without additional information. In the present experiments, the use of a spin-polarized primary electron beam, coupled with energy- and angle-resolved polarization analysis of the scattered electrons, is shown to provide new insights into the dynamics of electron energy loss at surfaces and the relative contributions of the different inelastic-scattering channels to the total energy-loss spectrum.

### II. ENERGY-LOSS MECHANISMS AND SCATTERING MODEL

Inelastic scattering of electrons from crystalline surfaces is usually treated theoretically as a superposition of contributions from dipole scattering and impact scattering, though strictly speaking these represent the two limiting cases of an as yet unrealized fully microscopic description of the electron-surface interaction.<sup>1,2</sup> Dipole scattering arises as a consequence of the Coulomb interaction between incoming electrons and electric-field fluctuations set up in the vacuum outside the target by oscillating surface- and near-surface atoms.<sup>1,2</sup> These fluctuations are associated with elementary excitations of the medium, such as surface plasmon and/or intra/interband (electron-hole pair) excitations. (We disre-

gard phonon excitations which produce energy losses in the millielectronvolt range, well below those of interest here.) Dipolar processes occur well outside the target surface, where the electrons undergo predominantly small-angle scattering either preceded or followed by elastic scattering from the surface. Thus the dipole-scattered electrons are mostly concentrated within a small angle about the specular direction (and other Bragg directions). Because the inelastic scattering events occur in the vacuum at distances where there is insignificant wave function overlap with electrons in the target, there is no possibility of exchange, i.e., the incident and scattered electrons are one and the same.

However, incident electrons that penetrate the target (without having undergone dipole scattering) may be inelastically scattered in the near-surface region by short-range interactions, producing electron-hole pairs. Little is known, either experimentally or theoretically, about the angular distributions of such impact-scattered electrons as they emerge from the target, though it is often assumed that they are distributed over a broad range of angles with no preference for the specular scattering direction.<sup>1,2</sup> Electron-hole pair excitation via a short-range interaction makes possible exchange and the emerging electron may be either the one that was incident or one from the target.

We now consider in greater detail the effect of these scattering processes on the spin polarization of scattered electrons when the incident beam is spin polarized. Figure 1 illustrates schematically the inelastic direct and exchange channels accessible in electron-hole pair excitation by impact scattering from a paramagnetic target with equally populated spin-up ( $\uparrow$ ) and spin-down ( $\downarrow$ ) valence-band states. The spin-flip and non-spin-flip scattering rates corresponding to an inelastic energy loss  $\varepsilon$  and momentum transfer  $\mathbf{q}$  for, say, an incident spin-up ( $\uparrow$ ) electron can be expressed in terms of the amplitudes for the direct ( $f$ ) and exchange ( $g$ ) scattering channels diagrammed. In the case of direct scattering it is the incident electron that leaves the surface having suffered an inelastic energy loss, whereas for exchange scattering the emerging electron originates within the target. The spin-flip ( $F$ ) and non-spin-flip ( $N$ ) scattering rates are given by

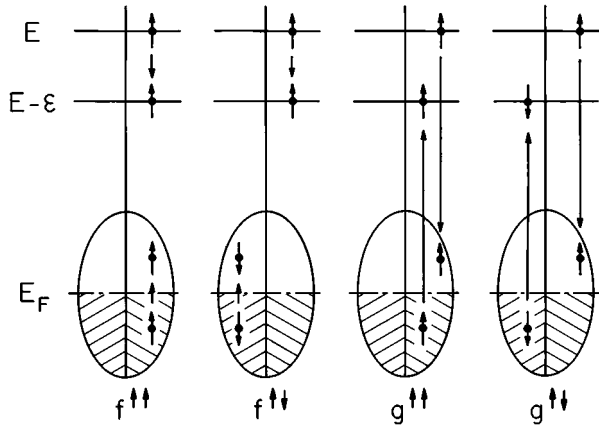


FIG. 1. Schematic representation of the inelastic direct and exchange-scattering channels important in the present work.

$$F(\varepsilon, \mathbf{q}) = \sum |g_{\uparrow\downarrow}(\varepsilon, \mathbf{q})|^2, \quad (1)$$

$$N(\varepsilon, \mathbf{q}) = \sum [ |f_{\uparrow\uparrow}(\varepsilon, \mathbf{q}) - g_{\uparrow\uparrow}(\varepsilon, \mathbf{q})|^2 + |f_{\uparrow\downarrow}(\varepsilon, \mathbf{q})|^2 ], \quad (2)$$

where the summations are over states for which energy and momentum are conserved. If it is assumed that the transition matrix elements coupling occupied and unoccupied states are independent of energy and constant over the Brillouin zone, the spin-flip and non-spin-flip scattering rates  $F(\varepsilon, \Theta_s)$  and  $N(\varepsilon, \Theta_s)$ , respectively, for inelastic energy loss  $\varepsilon$  and scattering angle  $\Theta_s$  may be written<sup>3</sup>

$$\begin{aligned} F(\varepsilon, \Theta_s) &= |M_F(\Theta_s)|^2 \int_{E_F-\varepsilon}^{E_F} n_0(E) n_u(E+\varepsilon) dE \\ &= |M_F(\Theta_s)|^2 J(\varepsilon), \end{aligned} \quad (3)$$

$$\begin{aligned} N(\varepsilon, \Theta_s) &= |M_N(\Theta_s)|^2 \int_{E_F-\varepsilon}^{E_F} n_0(E) n_u(E+\varepsilon) dE \\ &= |M_N(\Theta_s)|^2 J(\varepsilon), \end{aligned} \quad (4)$$

where  $E_F$  is the Fermi energy,  $M_F(\Theta_s)$  and  $M_N(\Theta_s)$  are the effective (energy-independent) matrix elements for spin-flip and non-spin-flip scattering, and  $n_0$  and  $n_u$  are, respectively, the densities of occupied and unoccupied electronic states. Thus, in this limit, both  $F(\varepsilon, \Theta_s)$  and  $N(\varepsilon, \Theta_s)$  are directly proportional to the convoluted, or joint, density of occupied and unoccupied states, represented by the integral  $J(\varepsilon)$ .

The electron-spin polarization is defined as the ratio of the difference in the number of scattered electrons with spin-up ( $\uparrow$ ) and spin-down ( $\downarrow$ ), divided by their sum. Thus, in the present approximation, and assuming that the detected electrons have undergone only single energy-loss events, the po-

larization  $P_I$  of impact-scattered electrons for an incident-beam polarization  $P_0$  is simply

$$\begin{aligned} P_I(\Theta_s) &= P_0 \frac{N(\varepsilon, \Theta_s) - F(\varepsilon, \Theta_s)}{N(\varepsilon, \Theta_s) + F(\varepsilon, \Theta_s)} \\ &= P_0 \frac{|M_N(\Theta_s)|^2 - |M_F(\Theta_s)|^2}{|M_N(\Theta_s)|^2 + |M_F(\Theta_s)|^2}, \end{aligned} \quad (5)$$

which is less than  $P_0$  and independent of energy loss, though perhaps dependent upon  $\Theta_s$ . (It is important to note that differences in the polarization of the incident and emerging electrons is strictly a consequence of exchange processes—no electron undergoes a true spin flip, the probability of which is negligibly small during the very brief electron-surface interaction.)

Dipole and impact scattering both contribute to the total scattered electron signal. Dipole scattering, however, preserves the full polarization  $P_0$  of the incident beam because electron exchange cannot occur. Thus, dipole scattering provides a scattered electron distribution with polarization  $P_0$ , upon which is superimposed a distribution of lower polarization resulting from electron-hole pair excitation in impact scattering. Denoting the rate for dipole scattering as  $D(\varepsilon, \Theta_s)$ , the net polarization of the scattered electrons will be

$$\begin{aligned} P(\varepsilon, \Theta_s) &= P_0 \frac{D(\varepsilon, \Theta_s) + N(\varepsilon, \Theta_s) - F(\varepsilon, \Theta_s)}{D(\varepsilon, \Theta_s) + N(\varepsilon, \Theta_s) + F(\varepsilon, \Theta_s)} \\ &= P_0 \left[ 1 - \frac{2\alpha(\varepsilon, \Theta_s)}{1 + \beta(\varepsilon, \Theta_s)} \right], \end{aligned} \quad (6)$$

where

$$\alpha(\varepsilon, \Theta_s) = \frac{F(\varepsilon, \Theta_s)}{N(\varepsilon, \Theta_s) + F(\varepsilon, \Theta_s)} \quad (7)$$

is the fraction of impact scattering events that result in a spin flip, and

$$\beta(\varepsilon, \Theta_s) = \frac{D(\varepsilon, \Theta_s)}{N(\varepsilon, \Theta_s) + F(\varepsilon, \Theta_s)} \equiv c(\varepsilon, \Theta_s) \frac{D(\varepsilon, \Theta_s)}{J(\varepsilon)} \quad (8)$$

gives the relative weight of dipole and impact scattering.  $c(\Theta_s)$  is a proportionality constant. The measured polarization  $P(\varepsilon, \Theta_s)$  will approach  $P_0$  when dipole scattering is dominant and  $P_0(1 - 2\alpha)$  when impact scattering is dominant.

In the present work we explore the applicability of this simple scattering model to the analysis of measured polarization loss spectra from paramagnetic and unmagnetized ferromagnetic metal targets. The targets studied were selected to provide a wide range of joint densities  $J(\varepsilon)$  of occupied and unoccupied valence states. Because  $\beta(\varepsilon, \Theta_s)$  is inversely proportional to  $J(\varepsilon)$ ,  $P(\varepsilon, \Theta_s)$  is expected to decrease as  $J(\varepsilon)$  increases. Moreover, to the extent that dipole-scattered electrons are expected to be more tightly concentrated about the specular direction than are impact-scattered electrons, polarizations measured in specular scattering geometry should be larger than those for off-specular scattering.

Earlier comparative studies of polarized electron scattering on Mo(110) and Cu(100) surfaces undertaken in specular

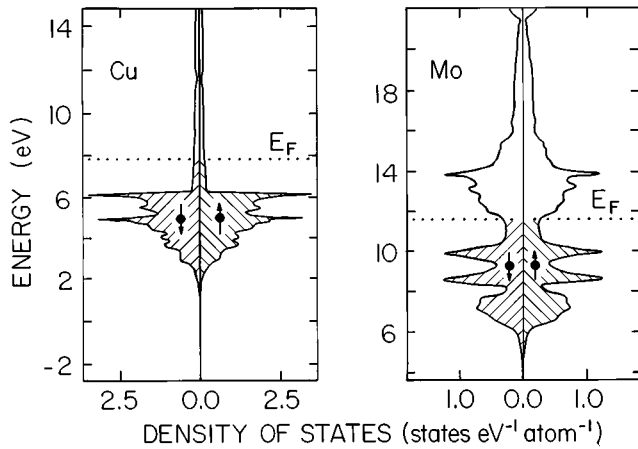


FIG. 2. Densities of states for Cu and Mo (taken from Ref. 4).

geometry have demonstrated that the scattered electron polarization is dependent on the joint density of states  $J(\epsilon)$  appropriate to the target.<sup>4</sup> As illustrated in Fig. 2, molybdenum has high densities of both occupied and unoccupied states whereas copper, with its closed  $d$  shell, has very few unoccupied states. Thus, for energy losses  $\leq 6$  eV,  $J(\epsilon)$  is much larger for molybdenum than for copper which correlates with the greater reduction in the scattered electron polarization observed experimentally. The present work extends these investigations of molybdenum and copper to include measurements in off-specular geometry, and a number of new targets, specifically silver, and iron and cobalt epitaxial films. As shown in Fig. 3, these targets provide a broad range of joint densities of states  $J(\epsilon)$ .<sup>5</sup> In the case of iron and cobalt, which were left unmagnetized, the densities of majority and minority states were summed before calculating  $J(\epsilon)$ .<sup>6</sup> (For cobalt, film growth results in a fcc structure for which the density of states is not available. The data

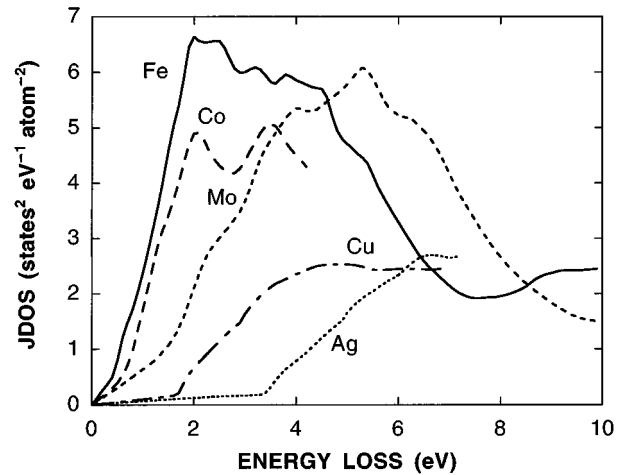


FIG. 3. Calculated joint densities of states  $J(\epsilon)$  for the targets investigated. Calculations for Ag, Co, and Cu do not extend to higher-energy losses because densities of high-lying unoccupied states were not available in Ref. 5.

in Fig. 3 were calculated using the density of states for the stable hcp structure.) The present targets provide a comprehensive test of the scattering model described earlier. As will be shown, the data suggest that dipole scattering dominates for the noble metals but that for targets with incompletely filled  $d$  shells, i.e., large  $J(\epsilon)$ , impact scattering can also be sizable. Further, the analysis indicates that single electron-hole pair excitation is the dominant energy-loss mechanism in impact scattering, which, like dipole scattering, tends to be concentrated in the specular direction.

### III. EXPERIMENTAL PROCEDURE

The present apparatus is shown schematically in Fig. 4. A collimated beam of spin-polarized electrons is directed at the

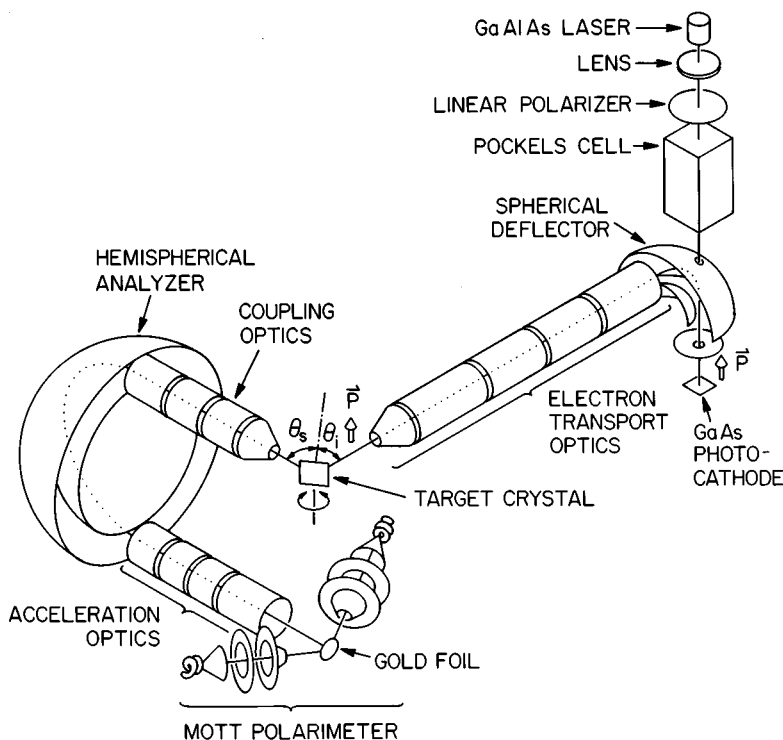


FIG. 4. Schematic diagram of the experimental apparatus.

target surface and the polarization of elastically/inelastically scattered electrons is measured as a function of energy and angle using a movable retarding-potential Mott polarimeter that is equipped with a hemispherical energy analyzer. The polarized electron beam is produced by photoemission from a cesiated GaAs surface using circularly polarized radiation from a  $\text{Ga}_{1-x}\text{Al}_x\text{As}$  laser.<sup>7</sup> The photoelectrons, which are initially longitudinally polarized, are accelerated and directed through a  $90^\circ$  electrostatic deflector. The emergent beam, now transversely polarized, passes through a series of electrostatic lenses and is then focused on the target surface at an angle of incidence  $\Theta_i$ . The polarization of  $P_0$  of the beam is  $\sim 0.26$  and can be simply reversed,  $P_0 \rightarrow -P_0$  by changing the sense of circular polarization of the radiation incident on the GaAs photocathode. The energy of the primary beam is 27 eV for all data presented.

Electrons leaving the target surface in a narrow range of angles ( $\sim \pm 3^\circ$ ) about the mean scattering angle  $\Theta_s$ , measured relative to the surface normal, enter a hemispherical energy analyzer that has an energy resolution of  $\sim 0.3$  eV. The polarization of the incident electrons is perpendicular to the scattering plane defined by the incident and scattered electrons. Those electrons transmitted through the hemispherical energy analyzer enter a low-energy Mott polarimeter<sup>8</sup> where the average component of their spin polarization perpendicular to the scattering plane is determined by measuring the left-right asymmetry that results because of the spin-orbit effect when the electrons (at 18 keV) are quasielastically scattered through  $\pm 120^\circ$  at a thorium surface. In practice, to eliminate instrumental asymmetries, the scattering asymmetry is determined with the incident electrons polarized both spin up and spin down. Ancillary measurements showed that for the surfaces and energies studied in the present work the scattered-electron currents were essentially independent of the spin of the incident electrons (the asymmetries were  $< 0.01$ ) and that the polarization of the scattered electrons produced by an unpolarized incident beam was unobservably small. It was also verified that for all targets the polarization of elastically scattered electrons was equal to that of the incident electron beam. These observations indicate that spin-orbit effects do not play an important role in determining the polarization of the scattered electrons. It is therefore reasonable to assume that the polarization of the scattered electrons is simply proportional to the polarization  $P_0$  of the incident beam and will reverse sign when  $P_0$  is reversed. In this event, the polarization of the scattered electrons is given by<sup>4,8</sup>

$$P = \frac{1}{S_{\text{eff}}} \frac{X-1}{X+1}, \quad (9)$$

where  $S_{\text{eff}}$  is the magnitude of the analyzing power (effective Sherman function) and  $X = (R_L R'_R / R_R R'_L)^{1/2}$ .  $R_L(R'_L)$  and  $R_R(R'_R)$  are the count rates in the two detection channels, labeled left and right, with incident-beam polarization  $P_0(-P_0)$ .

The single-crystal Cu(100) and Ag(100) surfaces were cleaned by repeated cycles of  $\text{Ar}^+$ -ion bombardment and thermal annealing until the contamination level was determined to be  $< 1\%$  by Auger electron analysis. These surfaces

exhibited sharp low-energy electron-diffraction (LEED) patterns. The molybdenum, iron, and cobalt surfaces were prepared by epitaxially growing several monolayers on the Cu(100) substrate using electron-beam evaporators. The structure and quality of the films were verified by LEED measurements which exhibited well-defined patterns and low diffuse background. Contamination levels were below 1%.

#### IV. EXPERIMENTAL RESULTS AND ANALYSIS

Angle- and energy-resolved intensity distributions of electrons elastically and inelastically scattered from Cu(100), Mo/Cu(100), and from unmagnetized Co/Cu(100) surfaces are shown in Fig. 5 and are representative of those measured with all the present targets. The scattering geometry is indicated in the inset. The primary beam energy in each case was 27 eV. It is seen that the angular distributions are sharper for clean Cu(100) than for the epitaxial films, presumably as a result of imperfect growth. Nonetheless, for all targets inelastically scattered electrons with relatively small energy loss tend to be concentrated in the specular direction, but the distributions broaden as the energy loss increases. These observations are consistent with general expectations based on the discussion of dipole and impact scattering in Sec. II. The energy-resolved intensity distributions of electrons scattered off-specular from both the Cu(100) and Mo/Cu(100) surfaces are shown in Fig. 6. The scattered intensity is least for energy losses  $\lesssim 1$  eV, and gradually increases with increasing energy loss. Similar behavior is observed both on and off specular with all targets.

The polarization  $P$  of the backscattered electrons, normalized to that of the incident electron beam ( $P_0 = 0.26$ ), is shown as a function of inelastic energy loss in Fig. 7 for each of the five targets studied.<sup>9</sup> The data include polarization spectra obtained for both specular and off-specular scattering, with scattering geometries indicated in the insets. The majority of the data were recorded at an angle of incidence of  $35^\circ$  and at a nonspecular scattering angle of  $55^\circ$ , i.e.,  $20^\circ$  off specular. However, as suggested by the data for Fe/Cu(100), which was taken at an angle of incidence of  $55^\circ$  and a nonspecular scattering angle of  $35^\circ$ , the observed effects appear to be relatively insensitive to the off-specular scattering geometry, i.e., whether toward or away from the surface normal. The behavior observed for specular scattering from Cu(100) and Mo/Cu(100) is similar to that noted in earlier studies.<sup>4,10</sup> Inspection reveals that the decreases observed in the scattered electron polarization, i.e.,  $P/P_0$ , are correlated qualitatively with the joint densities of states  $J(\epsilon)$  shown in Fig. 3. Also, the measured polarizations are systematically larger for specular than for nonspecular scattering, which is expected, at least qualitatively, because the (fully polarized) dipole-scattered electrons are concentrated in the specular direction. However, the polarization differences are not large. This suggests that the impact-scattered electrons also tend to be peaked in the specular direction, though not so strongly as for dipole scattering.

Figure 8 shows the polarizations  $P/P_0$  predicted by the present model, i.e., Eq. (6), as a function of the ratio  $\beta$  of the dipole to impact-scattering rates for several values of the parameter  $\alpha$  that represents the fraction of impact-scattering events that result in exchange. The value  $\alpha = 1/4$  is obtained

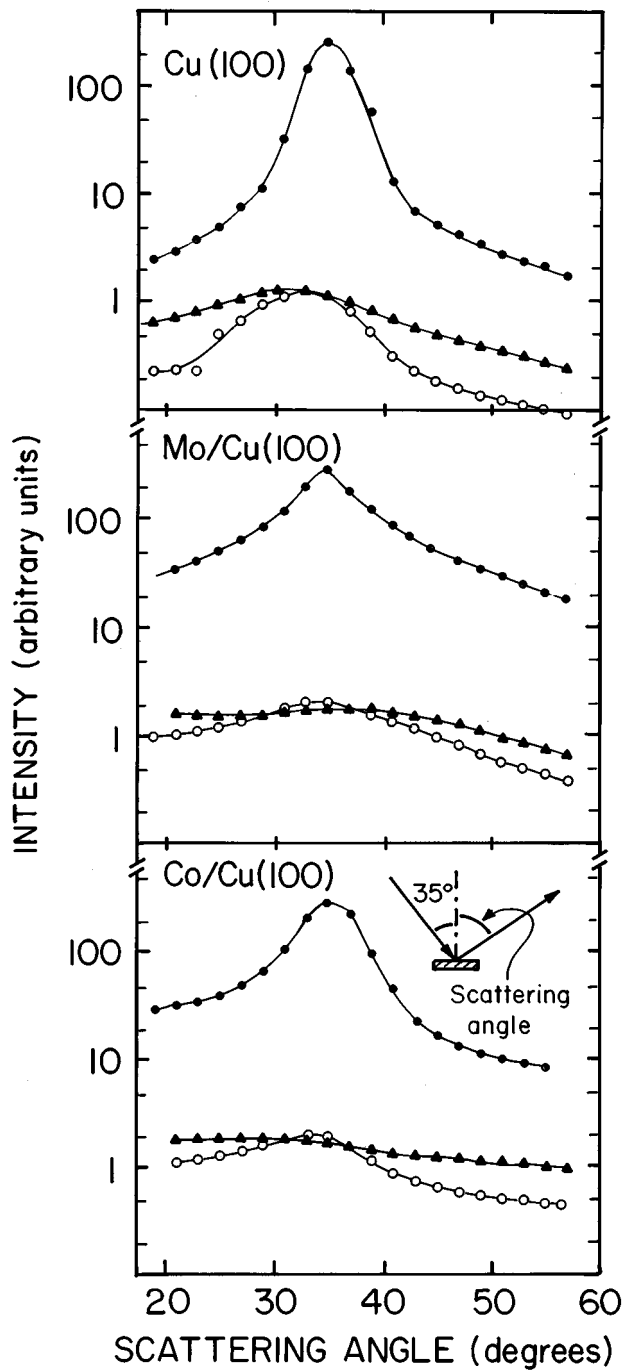


FIG. 5. Angle- and energy-resolved distributions of electrons elastically (●) and inelastically (○,  $\epsilon=2$  eV; ▲,  $\epsilon=6$  eV) scattered from Cu(100), Mo/Cu(100), and unmagnetized Co/Cu(100) surfaces. The scattering geometry is indicated in the inset.

by assuming that the rate  $N$  associated with direct non-spin-flip scattering is three times that for spin-flip exchange scattering,  $F$ . This would be expected if the rates associated with each of the (three) possible nonflip channels were equal and if interference between direct and exchange channels is not important. Interference effects, however, might reduce the total rate for direct scattering and the assumption that the rates for direct and exchange scattering are equal leads to  $\alpha=1/2$ . It appears reasonable to expect that the true value of  $\alpha$  will lie in the range  $\frac{1}{4}$  to  $\frac{1}{2}$ , i.e., in the shaded region

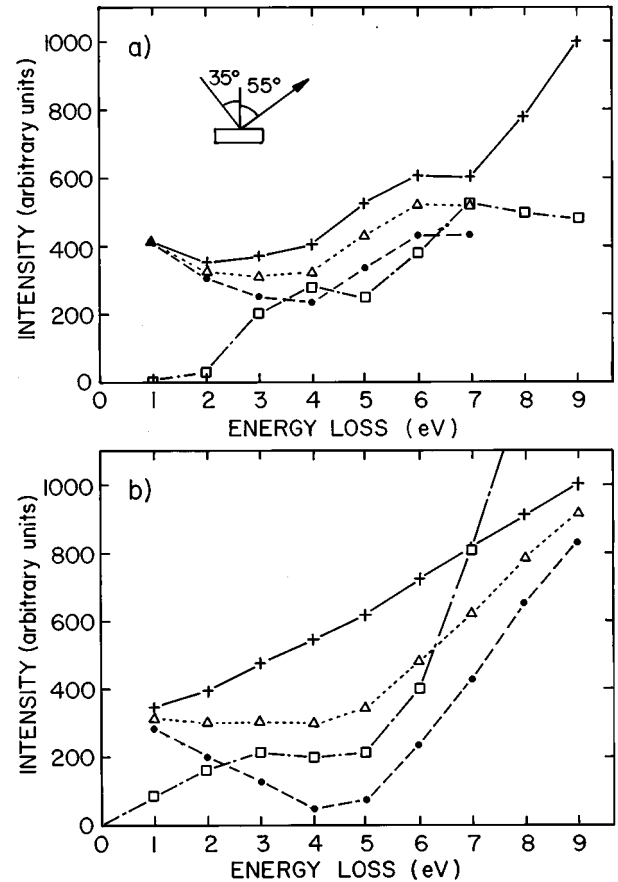


FIG. 6. Energy distributions of electrons scattered nonspecularly from (a) Cu(100) and (b) Mo/Cu(100) surfaces. +, total scattered electron current  $I(\epsilon)$ ; ●,  $\Delta$  contributions  $I_D(\epsilon)$  associated with dipole scattering calculated using Eq. (20) assuming  $\alpha(\epsilon)=0.25$  and 0.5, respectively; □, energy dependence of the dipole-scattered current predicted using the complex dielectric function  $d(\epsilon,0)$ . The scattering geometry is indicated in the inset.

indicated in Fig. 8. The limiting case  $\alpha=1$ , which corresponds to all impact scattering being associated with exchange, is also included.

Inspection of the data for Cu and Ag in Fig. 7 shows that, for inelastic energy losses,  $\leq 6$  eV, the measured values of  $P/P_0$  lie in the range  $\sim 0.8-0.95$ , even including the off-specular data. As evident from Fig. 8, such values of  $P/P_0$  imply ratios  $\beta$  of dipole to impact scattering of  $\sim 2-20$ , indicating that for these elements dipole scattering is dominant. This is not surprising because each has a filled  $3d$  shell leading to small joint densities  $J(\epsilon)$  of occupied and unoccupied states, especially for small inelastic energy losses (see Fig. 3). In contrast, values of  $P/P_0 \leq 0.6$  are measured for Mo/Cu(100), Fe/Cu(100), and Co/Cu(100) which, as suggested by Fig. 8, can only be obtained if the rate for impact scattering is greater than, or at least comparable to, that for dipole scattering, i.e., if  $\beta \leq 1$ . This can be accounted for because these materials have large densities of unoccupied states making  $J(\epsilon)$  large.

Several tests of the validity and of the internal self-consistency of the present model can be made by considering the separate contributions of dipole and impact scattering to the measured scattered electron current  $I(\epsilon)$  at some fixed

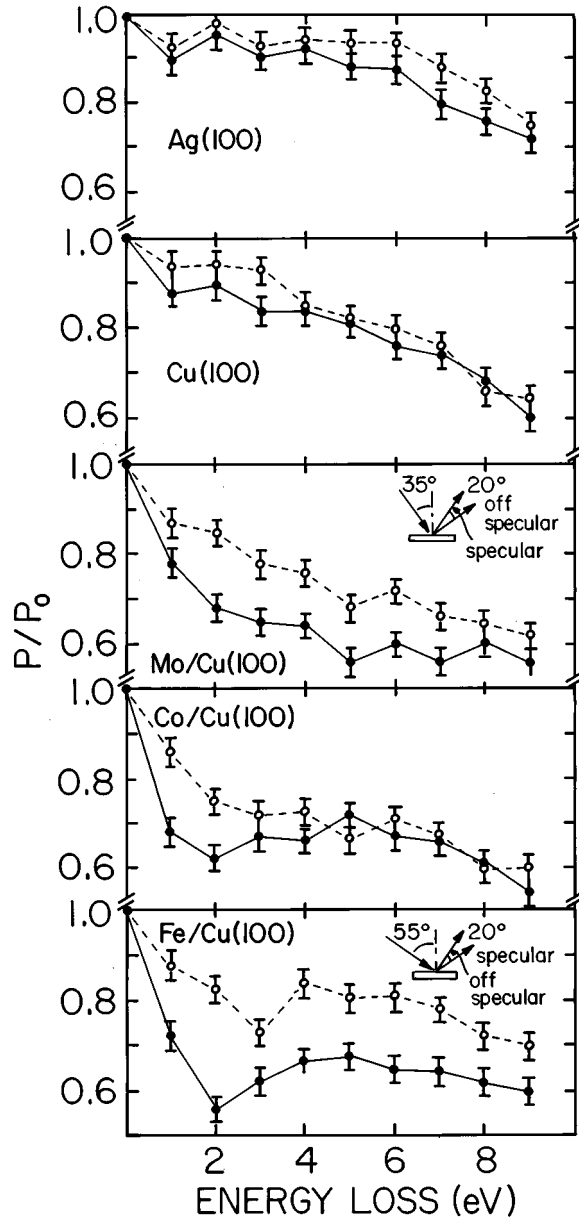


FIG. 7. Normalized polarization of electrons scattered specularly ( $\circ$ ) and nonspecularly ( $\bullet$ ) from each of the five targets investigated, as a function of inelastic energy loss. Scattering geometries are indicated in the insets.

scattering angle. Denoting these contributions by  $I_D(\varepsilon)$  and  $I_{N+F}(\varepsilon)$ , respectively, their ratio  $\beta$  is given from Eq. (6) by

$$\beta(\varepsilon) = \frac{I_D(\varepsilon)}{I_{N+F}(\varepsilon)} = \frac{2\alpha(\varepsilon)}{1 - P(\varepsilon)/P_0} - 1, \quad (10)$$

where  $\alpha(\varepsilon)$  is the fraction of impact-scattering events that lead to a spin flip. Consider initially the use of the model and the measured scattered electron energy distributions to predict the energy dependence of the scattered electron polarization  $P(\varepsilon)$ . This can be accomplished by first calculating the contribution to the total scattered electron current due to impact scattering at some particular inelastic energy loss  $\varepsilon_r$ , which is given by

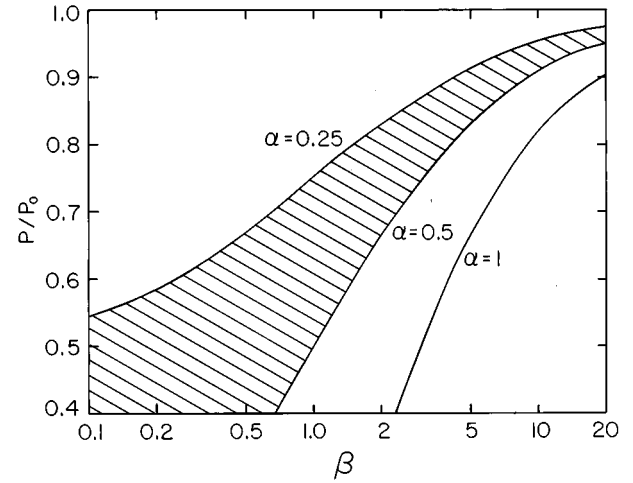


FIG. 8. Normalized polarizations predicted by Eq. (6), as a function of the ratio  $\beta$  of dipole- to impact-scattering rates, for several values of the parameter  $\alpha$  that represents the fraction of impact-scattering events that result in electron exchange.

$$I_{N+F}(\varepsilon_r) = I(\varepsilon_r) - I_D(\varepsilon_r) = \frac{I(\varepsilon_r)}{1 + \beta(\varepsilon_r)}, \quad (11)$$

where  $\beta(\varepsilon_r)$  is related, through Eq. (10), to the measured scattered electron polarization  $P(\varepsilon_r)$  at  $\varepsilon_r$ . If it is further assumed that, as discussed previously, impact-scattering rates are proportional to the joint density  $J(\varepsilon)$  of occupied and unoccupied states, this current  $I_{N+F}(\varepsilon_r)$  can be used to estimate the currents due to impact scattering at other energies via

$$I_{N+F}(\varepsilon) = \frac{J(\varepsilon)}{J(\varepsilon_r)} I_{N+F}(\varepsilon_r). \quad (12)$$

Denoting the ratio  $J(\varepsilon)/J(\varepsilon_r)$  by  $J_n(\varepsilon)$ ,  $I_{N+F}(\varepsilon)$  can be written

$$I_{N+F}(\varepsilon) = \frac{J_n(\varepsilon)I(\varepsilon_r)}{1 + \beta(\varepsilon_r)}, \quad (13)$$

whence the current associated with dipole scattering is given by

$$I_D(\varepsilon) = I(\varepsilon) - I_{N+F}(\varepsilon) = I(\varepsilon) - \frac{J_n(\varepsilon)I(\varepsilon_r)}{1 + \beta(\varepsilon_r)}. \quad (14)$$

The ratio of these currents then provides an expression for the value of  $\beta(\varepsilon)$  to be expected at all inelastic energy losses  $\varepsilon$ , i.e.,

$$\beta(\varepsilon) = \frac{I_D(\varepsilon)}{I_{N+F}(\varepsilon)} = \frac{I(\varepsilon)[1 + \beta(\varepsilon_r)]}{I(\varepsilon_r)J_n(\varepsilon)} - 1. \quad (15)$$

$\beta(\varepsilon_r)$  may be written in terms of the (measured) electron polarization  $P(\varepsilon_r)$  using Eq. (10), yielding

$$\beta(\varepsilon_r) = \frac{2\alpha(\varepsilon_r)}{1 - P(\varepsilon_r)/P_0} - 1. \quad (16)$$

Substitution in Eq. (15) gives

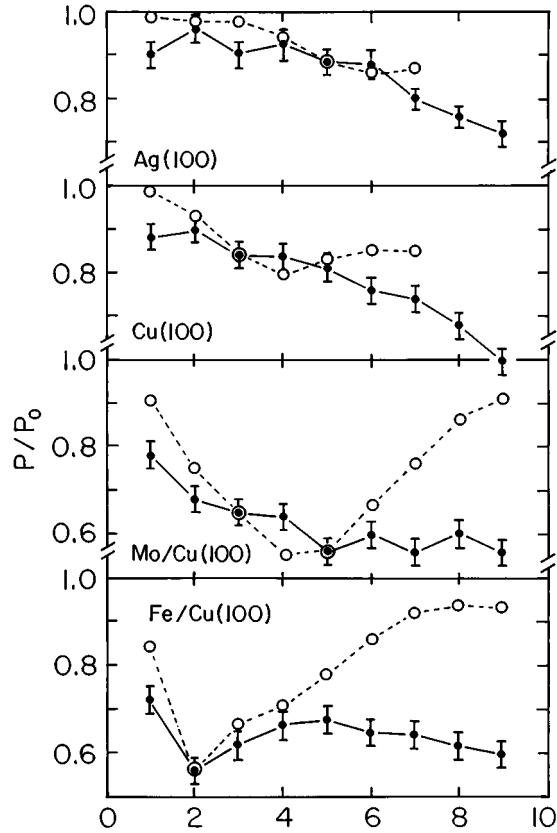


FIG. 9. Comparison between the measured off-specular polarizations (●) and predictions based on Eq. (19) (○).

$$\beta(\varepsilon) = \frac{I(\varepsilon)2\alpha(\varepsilon_r)}{I(\varepsilon_r)J_n(\varepsilon)[1 - P(\varepsilon_r)/P_0]} - 1. \quad (17)$$

Use of this relation, coupled with Eq. (6), provides an expression for the expected energy dependence of the scattered electron polarization

$$\frac{P(\varepsilon)}{P_0} = 1 - \frac{2\alpha(\varepsilon)}{1 + \beta(\varepsilon)} = 1 - \frac{I(\varepsilon_r)J_n(\varepsilon)\alpha(\varepsilon)[1 - P(\varepsilon_r)/P_0]}{I(\varepsilon)\alpha(\varepsilon_r)}. \quad (18)$$

The energy dependence of the fraction  $\alpha(\varepsilon)$  of impact-scattering events that result in a spin flip is not known. It appears reasonable to expect, however, that this fraction will not be strongly energy dependent. If it is assumed as a first approximation that  $\alpha(\varepsilon)$  is energy independent, Eq. (18) reduces to

$$\frac{P(\varepsilon)}{P_0} = 1 - \frac{I(\varepsilon_r)J_n(\varepsilon)[1 - P(\varepsilon_r)/P_0]}{I(\varepsilon)}. \quad (19)$$

Values of  $P(\varepsilon)/P_0$  obtained using this expression are included in Fig. 9. The data for Fe/Cu(100) and Mo/Cu(100) were derived using reference energies  $\varepsilon_r$  of 2 and 5 eV, respectively. These energies were selected because they lie close to the minima in the observed polarization profiles and because they correspond to regions where  $P(\varepsilon)$  is large. Reference energies of 3 and 5 eV were employed for Cu(100) and Ag(100), respectively, and represent the energies at which  $J(\varepsilon)$  for these targets first becomes large. The values

of  $P(\varepsilon)/P_0$  derived from Eq. (19) are in reasonable agreement with the experimental observations, at least for inelastic energy losses  $\leq 6$  eV. Agreement becomes less good for larger energy losses, possibly as a consequence of the increasing importance of multiple scattering. Nonetheless, the general level of agreement evident in Fig. 9 suggests that the present model and the assumptions inherent in deriving Eq. (19) are at least reasonable.

A further test of the present model can be obtained by considering the energy dependence of the contribution  $I_D(\varepsilon)$  to the total scattered electron current due to dipole scattering which, using Eqs. (10) and (14), can be written

$$I_D(\varepsilon) = I(\varepsilon) - J_n(\varepsilon) \frac{I(\varepsilon_r)[1 - P(\varepsilon_r)/P_0]}{2\alpha(\varepsilon_r)}. \quad (20)$$

Although the value of  $\alpha(\varepsilon_r)$  is not known, it is reasonable to expect that, as discussed earlier, it will lie in the range 0.25–0.5. Values of  $I_D(\varepsilon)$  derived using Eq. (2) and these two values of  $\alpha(\varepsilon_r)$  are included in Fig. 6. Note that, as discussed earlier, for Cu(100) dipole scattering is dominant, whereas for Mo/Cu(100) impact scattering provides a major contribution to the scattered electron signal.

The rate for dipole scattering at a solid surface is thought to be governed by the complex dielectric function  $d(\varepsilon, \mathbf{q})$  and to be proportional to  $\text{Im}\{-1/[1 + d(\varepsilon, \mathbf{q})]\}$ , the surface energy-loss function.<sup>2,11,12</sup> In the limit of zero-momentum transfer, i.e.,  $\mathbf{q} = \mathbf{0}$ , the dielectric function is related to the dielectric constant  $n(\varepsilon)$  and extinction coefficient  $k(\varepsilon)$  by

$$d(\varepsilon) = [n(\varepsilon) - ik(\varepsilon)]^2 = d_1(\varepsilon) + id_2(\varepsilon), \quad (21)$$

where

$$d_1(\varepsilon) = n(\varepsilon)^2 - k(\varepsilon)^2,$$

$$d_2(\varepsilon) = 2n(\varepsilon)k(\varepsilon).$$

Values of  $n(\varepsilon)$  and  $k(\varepsilon)$  for several of the targets studied in this work are tabulated in the literature<sup>13</sup> and can be used to obtain an estimate of the energy dependence of the dipole-scattered signal. This predicted energy dependence is included in Fig. 6 and is seen to be in qualitative agreement, at least for inelastic energy losses  $\varepsilon \leq 6$  eV, with that obtained using Eq. (20), again pointing to the essential correctness of the present model.<sup>14</sup>

## V. SUMMARY AND CONCLUSIONS

The present work suggests that electron-spin labeling techniques can be used to examine the relative importance of dipole and impact scattering in inelastic electron scattering from surfaces. The polarization of incident electrons is fully preserved in the case of dipole scattering, but is degraded by exchange reactions in the case of impact scattering. Consideration of the data using a simple model indicates that for targets such as Ag or Cu that have filled 3d-shells dipole scattering is dominant, whereas for targets like Mo, Fe, and Co with large densities of unoccupied states the rate for impact scattering is greater than, or comparable to, that for dipole scattering for inelastic energy losses  $\varepsilon \geq 1$  eV. Further analysis suggests that for each target the rate for impact scattering is approximately proportional to the joint density

$J(\epsilon)$  of occupied and unoccupied states. It is also observed that impact-scattered electrons tend to be concentrated near the specular direction, but not so strongly as dipole-scattered electrons. This suggests that in impact-scattering electron-hole pair excitation occurs predominantly via relatively small-angle inelastic scattering events either preceded or followed by elastic backscattering from the ion cores. Thus, since the angular distributions of impact-scattered electrons are governed primarily by the elastic event, it follows that there should be little difference in angular distributions of direct- and exchange-scattered electrons, i.e., the fraction of

impact-scattering events that lead to a spin flip should be approximately independent of  $\Theta$ .

#### ACKNOWLEDGMENTS

It is a pleasure to acknowledge valuable discussions with D. L. Mills and D. R. Penn during the course of this work, and to thank Richard Popple for assistance in the data analysis. This research is supported by the Office of Basic Energy Sciences, U. S. Department of Energy and the Robert A. Welch Foundation.

<sup>1</sup>D. L. Mills, *Surf. Sci.* **48**, 59 (1975).

<sup>2</sup>H. Ibach and D. L. Mills, *Electron Energy Loss Spectroscopy and Surface Vibrations* (Academic, New York, 1982), Chap. 3.

<sup>3</sup>D. R. Penn, S. P. Apell, and S. M. Girvin, *Phys. Rev. B* **32**, 7753 (1985).

<sup>4</sup>G. A. Mulhollan, X. Zhang, F. B. Dunning, and G. K. Walters, *Phys. Rev. B* **41**, 8122 (1990).

<sup>5</sup>Calculated using densities of states from D. A. Papaconstantopoulos, *Handbook of the Band Structure of Elemental Solids* (Plenum, New York, 1986).

<sup>6</sup>For an unmagnetized ferromagnetic target it is necessary to separately consider scattering from the different randomly oriented domains. Within a single domain, relative to the majority ( $\uparrow$ ) and minority ( $\downarrow$ ) spin directions, there are four different joint densities of states:  $J_{\uparrow\uparrow}$ ,  $J_{\downarrow\downarrow}$ ,  $J_{\uparrow\downarrow}$ , and  $J_{\downarrow\uparrow}$ . If it is assumed as a worse case scenario that domains are equally sampled whose magnetization is parallel and antiparallel to the incident electron spin, detailed analysis shows that under the assumptions leading to Eq. (5) the polarization of impact scattered electrons would be

$$P = \frac{|M_M|^2(J_{\uparrow\uparrow} + J_{\downarrow\downarrow}) - |M_F|^2(J_{\uparrow\downarrow} + J_{\downarrow\uparrow})}{|M_M|^2(J_{\uparrow\uparrow} + J_{\downarrow\downarrow}) + |M_F|^2(J_{\uparrow\downarrow} + J_{\downarrow\uparrow})}.$$

This reduces to Eq. (5) if  $J_{\uparrow\uparrow} + J_{\downarrow\downarrow} = J_{\uparrow\downarrow} + J_{\downarrow\uparrow}$ . Calculation of the separate  $J$ 's show that this is approximately true and that it is reasonable to apply Eq. (5) to an unmagnetized ferromagnetic sample using a simple summed joint density of states, especially considering the semiquantitative nature of the model.

<sup>7</sup>D. T. Pierce, R. J. Celotta, G.-C. Wang, W. N. Unertl, A. Galejs,

C. E. Kuyatt, and S. R. Mielczarek, *Rev. Sci. Instrum.* **51**, 578 (1980).

<sup>8</sup>F. C. Tang, X. Zhang, F. B. Dunning, and G. K. Walters, *Rev. Sci. Instrum.* **59**, 504 (1988).

<sup>9</sup>The off-specular polarization spectrum for Cu(100) is in marked disagreement with earlier work of K.-P. Kämper, D. L. Abraham, and H. Hopster, *Phys. Rev. B* **45**, 14 335 (1992), Fig. 6, who reported much greater polarization losses using a similar geometry and approximately the same primary beam energy as employed in the present work. They reported no measurements in specular geometry.

<sup>10</sup>Significantly higher polarizations were reported to Ref. 4 for energy losses in the range 8–10 eV (outside the range of interest of the present work). We cannot account for this discrepancy but the dispersive energy analyzer used in the present work greatly improves the signal-to-noise ratio of the measurements and reduces the possibility of systematic error.

<sup>11</sup>H. Frotzheim, H. Ibach, and D. L. Mills, *Phys. Rev. B* **11**, 4980 (1975).

<sup>12</sup>C. J. Powell, *Surf. Sci.* **299/300**, 34 (1994).

<sup>13</sup>*Handbook of Optical Constants of Solids*, edited by E. D. Palik (Academic, New York, 1986).

<sup>14</sup>The calculated loss functions  $\text{Im}\{-1/[1+d(\epsilon,0)]\}$  that are plotted in Fig. 6 do not take account of events involving momentum transfer; also, comparisons with experimental data are usually applied in specular geometry where dipole scattering is concentrated.